Chapter 1

Basic Framework

Buoyancy is induced by density variations that may occur due to gravity, as in planetary and stellar atmosphere, or due to temperature variation, as in thermal convection. In this chapter, we introduce the framework and equations for buoyancy-driven flows. In later chapters we will describe complex behaviour exhibited by such flows.

1.1 Equations in terms of density variation

A fluid flow is described using velocity, density, and energy variables. In this paper we focus on systems in which the density fluctuations is much smaller than its average value. We write the local density ρ_l (subscript l denotes *local*) as a sum of the density stratification $\bar{\rho}(z)$ and density fluctuation ρ:

$$\rho_l(x, y, z) = \bar{\rho}(z) + \rho(x, y, z). \tag{1.1}$$

It is customary to assume a linear density profile for $\bar{\rho}(z)$:

$$\bar{\rho}(z) = \rho_b + \frac{d\bar{\rho}}{dz} z = \rho_b + \frac{\rho_t - \rho_b}{d} z, \tag{1.2}$$

where ρ_b, ρ_t are respectively the densities at the bottom and top layers that are separated by distance d (see Fig. 1.1). The top and bottom layer may be embedded in a larger flow, or they could be plates maintaining the above density. The latter system has a boundary layer, but former one does not.

We assume that the gravity is downward, along $-\hat{z}$. Hence the gravitational force density on the fluid is

$$\begin{aligned} \mathbf{F}_g &= -g\rho_l \hat{z} = -g(\bar{\rho} + \rho)\hat{z} \\ &= -g\nabla \left(\int^z \bar{\rho}(z')dz' \right) - \rho g \hat{z}. \end{aligned} \tag{1.3}$$

The second term of the above expression, $-\rho g \hat{z}$, occurs due to the density variation of the fluid with relative to the local surrounding. This force is called

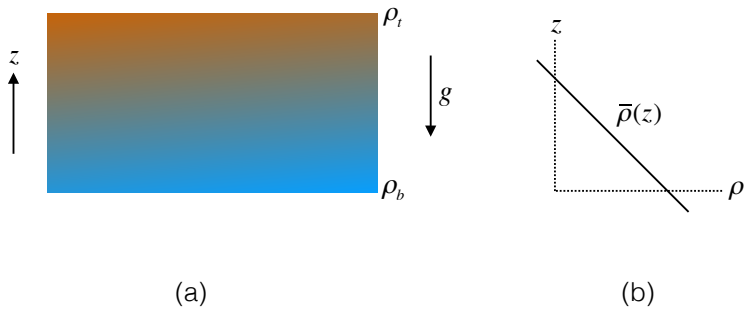

Figure 1.1: density...

buoyancy. It is along $-\hat{z}$ for $\rho > 0$, but along $\hat{z}$ for $\rho < 0$. We remark that the density variation could be caused by– strong gravity, for example in planetary and stellar atmospheres; or by temperature variations, as in thermal convection in which hotter (lighter) fluid ascend, and colder (heavier) fluid descends; or by infusion of soluble material, such as salt in ocean. We will discuss these systems in detail in later parts of the book.

A fluid flow is described by Navier Stokes equation

$$\rho_l \left[\frac{\partial \mathbf{u}}{\partial t} + (\mathbf{u} \cdot \nabla)\mathbf{u} \right] = -\nabla p + \mathbf{F}_g + \mu \nabla^2 \mathbf{u} + \mathbf{f}_u, \tag{1.4}$$

where $\mathbf{u}, p$ are respectively the velocity and pressure fields, $\mathbf{f}_u$ is the external force field in addition to the buoyancy, and μ is the dynamic viscosity of the fluid. Substitution of Eq. (1.3) in Eq. (1.4) yields

$$\rho_l \left[\frac{\partial \mathbf{u}}{\partial t} + (\mathbf{u} \cdot \nabla)\mathbf{u} \right] = -\nabla \sigma - \rho g \hat{z} + \mu \nabla^2 \mathbf{u} + \mathbf{f}_u, \tag{1.5}$$

where

$$\sigma = p + g \left(\int^z \bar{\rho}(z')dz' \right) \tag{1.6}$$

is the modified pressure. The continuity equation for the density yields

$$\frac{\partial \rho_l}{\partial t} + \nabla \cdot (\rho_l \mathbf{u}) = \nabla \cdot (\kappa \nabla \rho_l), \tag{1.7}$$

where κ is the diffusivity of the density. We assume that κ is constant in space and time. Equation (1.7) can be written as

$$\nabla \cdot \mathbf{u} = -\frac{1}{\rho_l} \frac{d\rho_l}{dt} + \frac{1}{\rho_l} \kappa \nabla^2 \rho_l. \tag{1.8}$$

Now we employ Oberbeck-Boussinesq (OB) approximation according to which the density of the fluid is approximately a constant, i.e., $(d\rho_l/dt)/\rho_l \approx 0$. Therefore, the relative magnitude of $\nabla \cdot \mathbf{u}$ would be

$$\frac{\nabla \cdot \mathbf{u}}{U/L} \approx \frac{L}{\rho_l U} \kappa \nabla^2 \rho_l \approx \frac{\kappa}{UL} = \frac{1}{\mathrm{Pe}}, \tag{1.9}$$

where L, U are the large length and velocity scales respectively, and Pe is the Péclet number. Typical buoyancy-driven flows have large Péclet number, hence we can assume $\nabla \cdot \mathbf{u} = 0$ for such flows, and replace ρ_l of Eq. (1.5) with the mean density of the fluid, ρ_m. Hence the governing equations for the buoyancy-driven flows are

$$\frac{\partial \mathbf{u}}{\partial t} + (\mathbf{u} \cdot \nabla)\mathbf{u} = -\frac{1}{\rho_m}\nabla\sigma - \frac{\rho}{\rho_m} g\hat{z} + \nu \nabla^2 \mathbf{u} + \mathbf{f}_u, \tag{1.10}$$

$$\frac{\partial \rho}{\partial t} + (\mathbf{u} \cdot \nabla)\rho = -\frac{d\bar{\rho}}{dz} u_z + \kappa \nabla^2 \rho, \tag{1.11}$$

$$\nabla \cdot \mathbf{u} = 0 \tag{1.12}$$

where $\nu = \mu/\rho_m$ is the kinematic viscosity. The assumption that ν, κ are constants in space and time is also considered to be a part of the OB approximation. It is important to note that even though fluid density is assumed to be an approximate constant in OB approximation, density variation is retained in the momentum equation for buoyancy-driven flows. We will show later the buoyancy is comparable to other terms of the momentum equation.

We will perform linear stability analysis of the above equations in Chapters 3 and 4 and show that the system is stable when $d\bar{\rho}/dz < 0$, and unstable when $d\bar{\rho}/dz > 0$. Flows with $d\bar{\rho}/dz < 0$ are called *stably-stratified flows*, and they have lighter fluid above the heavier fluid (see Fig. 1.2(a)). Such systems support waves in the linear limit, and nonlinear waves and turbulence in the nonlinear regime. In the presence of viscosity, the total energy of stably-stratified flows decays without $\mathbf{f}_u$, hence, $\mathbf{f}_u$ is employed to maintain a steady state. Examples of stably-stratified systems are Earth's atmosphere and ocean, where dense fluid sits below the lighter fluid. Note however that the density profile of the ambient atmosphere of a planet need not be linear; for the Earth, the density profile is exponential. The linear profile however is a good approximation for a small region of the atmosphere.

The second class of flows have $d\bar{\rho}/dz > 0$ (see Fig. 1.2(b)). Here heavier fluids sits above lighter ones. Such flows become unstable when $d\bar{\rho}/dz$ exceeds a critical value. For even larger nonlinearity, we obtain structures, chaos, and turbulence. Examples of such flows are Rayleigh-Bénard convection (RBC) and Rayleigh-Taylor instability. Note however that the background density of RBC varies linearly, but that of Rayleigh-Taylor instability exhibits a sharp jump.

As described earlier, temperature induces density variation, which yields buoyancy. We will discuss the governing equations in terms of velocity and temperature fields.

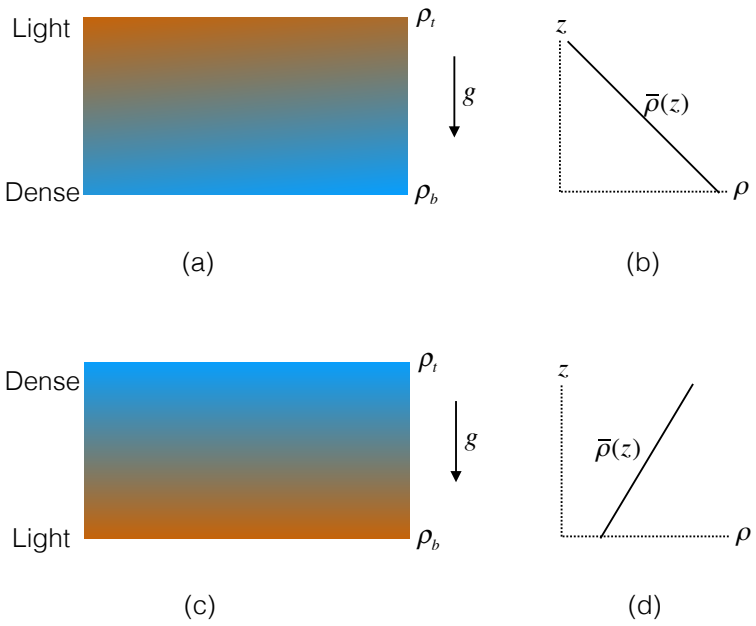

Figure 1.2: density.: stable, unstable.

1.2 Equations in terms of temperature

In a heated fluid, a hotter element is lighter than its colder counterpart. Lets us consider the background temperature profile to $\bar{T}(z)$. A fluid parcel with $T > \bar{T}(z)$ will be lighter that its background, and hence it will rise due to buoyancy. Opposite effect will happen to fluid element with $T < \bar{T}(z)$. In this section we will describe equation of motion of fluid in terms of temperature.

Here we consider a layer of fluid confined between two surfaces that are kept at temperature T_b and T_t, as shown in Fig. 1.3. If the system is inside a larger system, the top and bottom surfaces would be imaginary, and there would be no boundary layer. However, when the bounding are plates, then we obtain boundary layer.

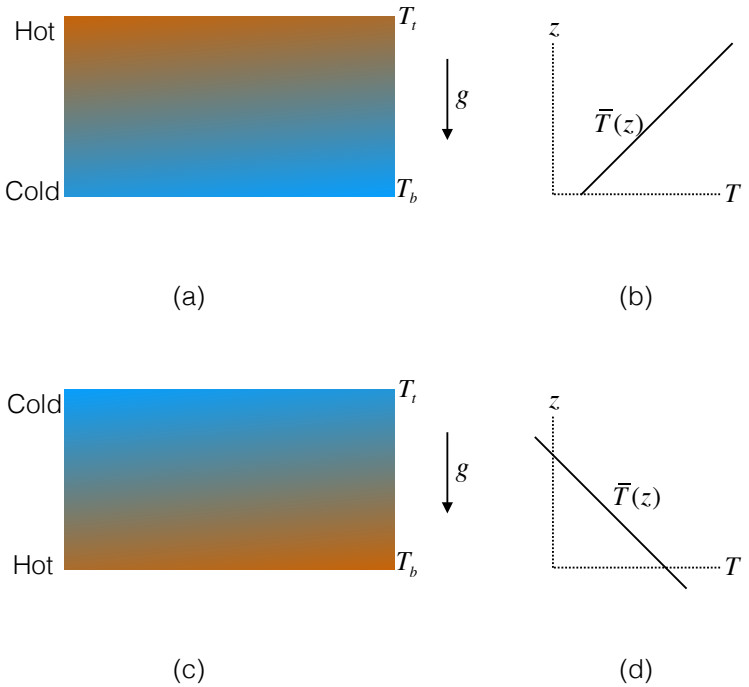

Figure 1.3: density...

We relate the temperature field T to the density ρ_l using a linear relationship

$$\rho_l = \rho_b \left[1 - \alpha(T - T_b)\right], \tag{1.13}$$

where α is the thermal expansion constant, which is assumed to be constant in space and time. In analogy with $\bar{\rho}$, we assume a linear temperature profile

$$\bar{T} = T_b + \frac{d\bar{T}}{dz} z = T_b - \frac{T_b - T_t}{d} z = T_b - \beta z. \tag{1.14}$$

It is customary to separate the temperature into the ambient temperature $\bar{T}$ and fluctuation θ over it:

$$T = \bar{T} + \theta. \tag{1.15}$$

A comparison of Eqs. (1.1, 1.13, 1.15) yields

$$\rho = -\rho_m \alpha \theta; \quad \frac{d\bar{\rho}}{dz} = -\alpha\beta, \tag{1.16}$$

substitution of which in Eqs. (1.10, 1.11) yields

$$\frac{\partial \mathbf{u}}{\partial t} + (\mathbf{u}\cdot\nabla)\mathbf{u} = -\frac{1}{\rho_m}\nabla\sigma + \alpha g\theta\hat{z} + \nu\nabla^2\mathbf{u}, \tag{1.17}$$

$$\frac{\partial \theta}{\partial t} + (\mathbf{u}\cdot\nabla)\theta = -\frac{d\bar{T}}{dz}u_z + \kappa\nabla^2\theta. \tag{1.18}$$

These equations coupled with

$$\nabla\cdot\mathbf{u} = 0 \tag{1.19}$$

are the governing equations for RBC.

In the above equation, we employ Oberbeck-Boussinesq approximation described in the previous section; namely, $|\rho|/\rho_m = \alpha|\theta| \ll 1$, and κ is constant in space and time. The OB approximation is applicable when the temperature difference between the two surfaces is not too large.

Equation (1.18) is also derived using the energy equation for fluids. The energy density per unit volume $\varepsilon = \rho C_v T$, and its evolution is [**?**]

$$\rho C_v \left[\frac{\partial T}{\partial t} + (\mathbf{u}\cdot\nabla)T\right] = -\nabla\cdot\mathbf{q} - p\nabla\cdot\mathbf{u} + \rho\epsilon_u \tag{1.20}$$

where $\mathbf{q}$ is the heat flux, C_v is the specific head at constant volume, and $\rho\epsilon_u$ is the kinetic energy dissipation rate per unit volume that enhances the internal energy. Under OB approximation, $\rho\epsilon_u$ is neglected in the energy equation. In the next section, we will illustrate this approximation for realistic situations. We also employ Fourier's law to model the heat flux:

$$\mathbf{q} = -K\nabla T \tag{1.21}$$

where K is the thermal conductivity.

For liquids like water, incompressibility condition yields $\nabla\cdot\mathbf{u} = 0$, substitution of which in Eq. (1.20) yields Eq. (1.18) with thermal diffusivity

$$\kappa = \frac{K}{\rho C_v}. \tag{1.22}$$

For gases, $p\nabla\cdot\mathbf{u}$ is comparable to the other terms of the energy equation:

$$p\nabla\cdot\mathbf{u} = -\frac{p}{\rho}\frac{D\rho}{Dt} = -\frac{p}{\rho}\left(\frac{\partial\rho}{\partial T}\right)_p \frac{DT}{Dt} = p\alpha\frac{DT}{Dt} \tag{1.23}$$

Here $\nabla \cdot \mathbf{u} \neq 0$, contrary to OB approximations. Now we assume the gas to be ideal, hence $p = \rho RT$, where R is the Rydberg's constant. Therefore,

$$\alpha = -\frac{1}{\rho}\left(\frac{\partial \rho}{\partial T}\right)_p = \frac{1}{T}. \tag{1.24}$$

Hence

$$p\nabla \cdot \mathbf{u} = \rho R \frac{DT}{Dt} = \rho(C_p - C_v)\frac{DT}{Dt} \tag{1.25}$$

where C_p, C_v are respectively the specific heats of the gas for constant pressure and constant volume. Substitution of the above in Eq. (1.20) yields Eq. (1.18) with $\kappa = K/(\rho C_p)$.

In the linear limit, Eqs. (1.17, 1.18) yield stable solution (e.g., waves) when $d\bar{T}/dz > 0$, and unstable solution when $d\bar{T}/dz < 0$. A major application with $d\bar{T}/dz < 0$ profile is Rayleigh-Bénard convection, which is the topic of the next section.

1.3 Rayleigh-Bénard convection

In general, thermally convective systems are quite complex involving complex geometries and complex material properties. A simplified model that captures essential features of thermal convection is called Rayleigh-Bénard convection (RBC) in which a fluid is confined between two thermally-conducting horizontal plates kept at constant temperatures T_b, T_t, as shown in Fig. XXX. Note that $d\bar{T}/dz < 0$. We employ Eqs. (1.17-1.19) to describe RBC. RBC is a major topic of this book.

RBC exhibits host of interesting phenomena depending on the temperature difference between the plates, which dictates the quantum of nonlinearity. First, the system is exhibits thermal instability when the temperature difference between the plates, $\Delta = T_b - T_t$ exceeds a critical value. Below this value, the heat is transported by conduction with a linear temperature profile

$$\bar{T}(z) = T_b - \beta z. \tag{1.26}$$

where

$$\beta = \frac{T_b - T_t}{d}. \tag{1.27}$$

The nonlinearity saturates the unstable growth, and we obtain convective rolls. When we increase Δ or nonlinearity, we obtain patterns, chaos, and turbulence. We will discuss these topics in the subsequent chapters of this book.

Most of the buoyancy-driven flows in the Earth's atmosphere and in engineering applications involve water, air, and oil, for which we list the parameters in Table 1. In the table we also list the parameters for Earth's mantle and helium gas. The ratio of ν and κ, called *Prandtl number* which is denote by Pr, plays an important role in the dynamics of RBC. Flows with large Pr tends to be dominated by the viscous term, and hence temperature fluctuations are

weaker in such flows. On the contrary, nonlinearity is stronger for small-Pr flows, hence such flows are more turbulent compared to large-Pr flows.

It is mathematically convenient to study limiting cases $\mathrm{Pr} \to \infty$ and $\mathrm{Pr} \to 0$. The former corresponds to finite κ and $\nu \to \infty$, while the latter to finite ν and $\kappa \to \infty$.

1.4 Justification of Oberbeck-Boussinesq approximation

As argued below, Oberbeck-Boussinesq approximation holds for these applications.

1. The parameters ν, κ, α are assumed to be constants. For water and air these constants vary within XXX % at normal temperature and pressure.

2. When the temperature difference between the plates $\Delta \leq 30\mathrm{C}$, we have $\rho/\rho_m \ll 1$ for typical fluids. For example, for water that has $\alpha \approx 3 \times 10^{-4}\mathrm{K}^{-1}$ at 30C, $\delta\rho/\rho_m = \alpha\Delta \approx 10^{-3}$ for $\Delta = 30\mathrm{C}$. Similarly for air at room temperature, $\alpha = 1/T = 1/300$ [Eq. (1.24)]. Hence, for a gas at $\Delta = 30\mathrm{C}$, $\delta\rho/\rho_m \approx 0.1$, which is relatively small.

3. As a result of item (2), the density of the flow is assumed to be constant, except for the buoyancy term ρg of the momentum equation. The density variation in the fluid causes buoyancy, which is comparable to the viscous term. We will demonstrate these comparisons during calculations of Rayleigh-Bénard instability (Chapter 4 and turbulent convection **??**.

4. The viscous dissipate rate ϵ_u is assumed to be small in BO approximation. For justification of this assumption, we estimate $\epsilon_u/(C_p(DT/Dt))$. In the viscous regime

$$\frac{\epsilon_u}{C_v(DT/Dt)} \approx \frac{\nu U^2/L^2}{\rho C_v U\Delta/L} \approx \frac{\nu U}{C_v L\Delta} \tag{1.28}$$

and in the turbulent regime

$$\frac{\epsilon_u}{C_v(DT/Dt)} \approx \frac{U^3/L}{C_v U\Delta/L} \approx \frac{U^2}{C_v L\Delta}. \tag{1.29}$$

We estimate $U \approx \sqrt{\alpha g \Delta d}$. For water, with $C_v = 4200\mathrm{J/kgK}$, $\Delta = 30$, $\nu = 10^{-6}\mathrm{m}^2/\mathrm{s}$, $\rho = 10^3\mathrm{kg/m}^3$, in the viscous regime

$$\frac{\epsilon_u}{C_v(DT/Dt)} \approx \frac{\nu U}{C_v L\Delta} \approx \frac{10^{-6} \times 10^{-1}}{4200 \times 30 \times 10^{-1}} \approx 10^{-11} \tag{1.30}$$

But in the turbulent regime,

$$\frac{\epsilon_u}{C_v(DT/Dt)} \approx \frac{U^2}{C_v L\Delta} \approx \frac{10^{-2}}{4200 \times 30 \times 10^{-1}} \approx 10^{-6} \tag{1.31}$$

Thus the viscous dissipation in the system is too small to be able to heat the fluid significantly. Hence we ignore ϵ_ν term in Eq. (1.20).

Thus we show that Oberbeck-Boussinesq approximation is valid for fluids at normal temperature and pressure. The above approximation however breaks down when Δ is too large, for example in planetary and stellar interiors. For such systems, we need to solve the equations of compressible fluids [Eqs. (1.5, 1.7)].

In the next section we will rewrite the equations for stably-stratified flows by transforming density into velocity variables.

1.5 Equations for stably-stratified flows simplified

The linearized version of Eqs. (1.10, 1.11) with $\nu = \kappa = 0$ are

$$\frac{\partial u_z}{\partial t} = \frac{\rho}{\rho_m} g, \tag{1.32}$$

$$\frac{\partial \rho}{\partial t} = -\frac{d\bar{\rho}}{dz} u_z, \tag{1.33}$$

The above set of equations can be rewritten as

$$\frac{\partial^2 u_z}{\partial t^2} = \frac{\rho}{\rho_m} \frac{d\bar{\rho}}{dz} u_z \tag{1.34}$$

whose solutions are waves with *Brunt-Väisälä frequency*:

$$N = \sqrt{\frac{g}{\rho_m} \left| \frac{d\bar{\rho}}{dz} \right|} \tag{1.35}$$

These waves are called *internal gravity waves* that will be discussed in more detail in Chapter 3.

Researchers often write the equation for stably-stratified flow in terms of variable

$$b = \frac{g}{N} \frac{\rho}{\rho_m}, \tag{1.36}$$

which has dimension of velocity [**?**]. In terms of b, Eqs. (1.10,1.11) become

$$\frac{\partial \mathbf{u}}{\partial t} + (\mathbf{u} \cdot \nabla)\mathbf{u} = -\frac{1}{\rho_m} \nabla\sigma - Nb\hat{z} + \nu\nabla^2 \mathbf{u}, \tag{1.37}$$

$$\frac{\partial b}{\partial t} + (\mathbf{u} \cdot \nabla) b = N u_z + \kappa \nabla^2 b. \tag{1.38}$$

The nondimensional parameters used for describing stably-stratified flows are

$$\text{Reynolds number Re} = \frac{|(\mathbf{u} \cdot \nabla)\mathbf{u}|}{|\nu\nabla^2 \mathbf{u}|} = \frac{u_{\text{rms}} d}{\nu}, \tag{1.39}$$

$$\text{Prandtl number Pr} = \frac{\nu}{\kappa}, \tag{1.40}$$

$$\text{Froude number Fr} = \frac{u_{\rm rms}/d}{N} = \frac{u_{\rm rms}}{dN}, \tag{1.41}$$

$$\text{Richardson number Ri} = \frac{N|b|_{\rm rms}}{|(\mathbf{u}\cdot\nabla)\mathbf{u}|} = \frac{N|b|_{\rm rms}d}{u_{\rm rms}^2}, \tag{1.42}$$

where $u_{\rm rms}$ is the rms velocity of flow, and $b_{\rm rms}$ is the rms value of b. Note that the Reynolds number is the ratio of the nonlinear term and viscous term, and the Richardson number is the ratio of the buoyancy and the nonlinear term. Froude number is the ratio of the frequencies associated with $u_{\rm rms}$ and gravity waves respectively.

Note that

$$\text{Ri} = \frac{N|b|_{\rm rms}d}{u_{\rm rms}^2} = \frac{1}{\text{Fr}^2}\frac{|b|_{\rm rms}}{Nd} = \frac{1}{\text{Fr}^2}\frac{\rho_{\rm rms}/d}{|d\bar{\rho}/dz|} \approx \frac{1}{\text{Fr}^2}. \tag{1.43}$$

This is an important relation which is used in describing nearly isotropic stably-stratified flows. We will describe later that strong gravity induces strong anisotropy that requires more parameters; we will describe them in Chapter **??**.

In the next section, we will describe Nondimensionalized equations of RBC.

1.6 Nondimensionalized versions of RBC equations

The equation for Rayleigh-Bénard convection are often presented in several nondimensionalized forms. These equations capture the relative strengths of various terms of the equations. Also, they help reduce the number of parameters of the system, which is quite useful for analysis, as well as for the numerical simulations and experiments.

RBC has two diffusive parameters ν and κ that yield two diffusive time scales: $\tau_\nu = d^2/\nu$ and $\tau_\kappa = d^2/\kappa$. Clearly $\tau_\nu < \tau_\kappa$ for $\text{Pr} > 1$, and vice versa for $\text{Pr} < 1$. It is customary, specially for numerical simulations, to resolve lower of the two time scales. Hence, we employ τ_ν as the time scale for $\text{Pr} > 1$, and τ_κ for $\text{Pr} < 1$. These choices become specially relevant for very large or very small Pr's.

Let us discuss the case when we use d^2/ν as the time scale. The other scales are: d for the length, κ/d for the velocity, $\Delta = |T_b - T_t|$ for the temperature, $\rho_m(\kappa/d)^2$ for the pressure. These quantities yield the following nondimensional variables:

$$\mathbf{u}' = \frac{\mathbf{u}}{(\kappa/d)}, \tag{1.44}$$

$$\mathbf{r}' = \frac{\mathbf{r}}{d}, \tag{1.45}$$

$$\nabla' = d\nabla \tag{1.46}$$

$$t' = \frac{t}{(d^2/\kappa)} \tag{1.47}$$

$$\sigma' = \frac{\sigma}{\rho_m(\kappa/d)^2} \tag{1.48}$$

$$\theta' = \frac{\theta}{\Delta} \tag{1.49}$$

In terms of the nondimensional variables, Eqs. (1.17,1.18) get converted to

$$\frac{\partial \mathbf{u}'}{\partial t'} + (\mathbf{u}' \cdot \nabla')\mathbf{u}' = -\nabla'\sigma' + \mathrm{RaPr}\theta'\hat{z} + \mathrm{Pr}\nabla'^2\mathbf{u}' \tag{1.50}$$

$$\frac{\partial \theta'}{\partial t'} + (\mathbf{u}' \cdot \nabla')\theta' = u_z' + \nabla'^2\theta', \tag{1.51}$$

where

$$\text{Rayleigh number Ra} = \frac{\alpha g d^3 \Delta}{\nu\kappa}, \tag{1.52}$$

and the Prandtl number Pr is defined in Eq. (1.40). Note that the ratio of the buoyancy and the viscous term is

$$\frac{\mathrm{RaPr}\theta_{\mathrm{rms}}}{\mathrm{Pr}\nabla^2 u_{\mathrm{rms}}} \approx \frac{\mathrm{Ra}}{k_{\mathrm{min}}^2}\frac{\theta_{\mathrm{rms}}}{u_{\mathrm{rms}}} \tag{1.53}$$

We will show in Chapter 4 that near the onset of Rayleigh-Bénard instability, $\mathrm{Ra} = 27\pi^4/(4k_{\mathrm{min}}^2)$, and $\theta_{\mathrm{rms}}/u_{\mathrm{rms}} \approx 1/k_{\mathrm{min}}^2$. Hence, near the instability, the aforementioned ratio is approximately 3. However, in the turbulent regime, the ratio of the buoyancy and the viscous term is more complex. However, broadly speaking, the Rayleigh number is some measure of the strength of the buoyancy with relative to the viscous term.

Note that we can also define the Rayleigh number in terms of density difference using the relation $|\rho_b - \rho_t|/\rho_m \approx \alpha\Delta$, which yields

$$\text{Rayleigh number Ra} = \frac{gd^3}{\nu\kappa}\frac{|\rho_b - \rho_t|}{\rho_m}. \tag{1.54}$$

For RBC with very small Pr, we take ν/d as the velocity scale, and d^2/ν as the time scale. In this limit, the diffusion term dominates $D\mathbf{u}/Dt$, and hence

$$\frac{\Delta}{d}u_z \approx \kappa\nabla^2\theta \Rightarrow \frac{\nu\Delta/d^2}{\sim}\frac{\kappa}{d^2}\theta. \tag{1.55}$$

Therefore

$$\theta \sim \frac{\nu}{\kappa}\Delta \to 0. \tag{1.56}$$

Consequently, for small Pr, we employ $(\nu/\kappa)\Delta$ as the scale for temperature fluctuations. In summary, for low Pr flows, the nondimensionalized variables

are

$$\mathbf{u}' = \frac{\mathbf{u}}{(\nu/d)}, \tag{1.57}$$

$$t' = \frac{t}{(d^2/\nu)} \tag{1.58}$$

$$\sigma' = \frac{\sigma}{\rho_m(\nu/d)^2} \tag{1.59}$$

$$\theta' = \frac{\theta}{\mathrm{Pr}\Delta}, \tag{1.60}$$

and the nondimensionalized equations in terms of these variables are

$$\frac{\partial \mathbf{u}'}{\partial t} + (\mathbf{u}' \cdot \nabla)\mathbf{u}' = -\nabla\sigma' + \mathrm{Ra}\theta'\hat{z} + \nabla^2\mathbf{u}', \tag{1.61}$$

$$\mathrm{Pr}\left(\frac{\partial \theta'}{\partial t} + (\mathbf{u}' \cdot \nabla)\theta'\right) = u_z' + \nabla^2\theta'. \tag{1.62}$$

For large Ra however the aforementioned nondimensional velocity becomes very large ($\sim \sqrt{\mathrm{RaPr}}$), which will be discussed in Chapter **??**. As a result, the time stepping for numerical integration ($(\delta x)/\sqrt{\mathrm{RaPr}}$, where δx is the grid size) becomes quite small. Hence, in numerical simulations, it is customary to employ $\sqrt{\alpha g \Delta d}$ as the velocity scale, which yields the following set of equations for moderate Pr:

$$\frac{\partial \mathbf{u}'}{\partial t} + (\mathbf{u}' \cdot \nabla)\mathbf{u}' = -\nabla\sigma' + \theta'\hat{z} + \sqrt{\frac{\mathrm{Pr}}{\mathrm{Ra}}}\nabla^2\mathbf{u}', \tag{1.63}$$

$$\frac{\partial \theta'}{\partial t} + (\mathbf{u}' \cdot \nabla)\theta' = Su_z' + \frac{1}{\sqrt{\mathrm{RaPr}}}\nabla^2\theta.' \tag{1.64}$$

As described earlier, for small Pr, temperature fluctuations are scaled using $\mathrm{Pr}\Delta$. Therefore, for small Pr, Eqs. (1.63, 1.64) get converted to

$$\frac{\partial \mathbf{u}'}{\partial t} + (\mathbf{u}' \cdot \nabla)\mathbf{u}' = -\nabla\sigma' + \mathrm{Pr}\theta'\hat{z} + \sqrt{\frac{\mathrm{Pr}}{\mathrm{Ra}}}\nabla^2\mathbf{u}', \tag{1.65}$$

$$\mathrm{Pr}\left(\frac{\partial \theta'}{\partial t} + (\mathbf{u}' \cdot \nabla)\theta'\right) = u_z' + \sqrt{\frac{\mathrm{Pr}}{\mathrm{Ra}}}\nabla^2\theta'. \tag{1.66}$$

In future discussion, for brevity we will drop the primes from the variables.

Another important nondimensional parameter for RBC is the Nusselt number Nu, which is the ratio of the total heat flux (convective plus conductive) and the conductive heat flux, and is computed using the following formula:

$$\mathrm{Nu} = \frac{-\kappa\nabla T_c + \langle u_z\theta\rangle}{-\kappa\nabla T_c} = \frac{\kappa\Delta/d + \langle u_z\theta\rangle}{\kappa\Delta/d}. \tag{1.67}$$

1.7 Boundary conditions, Box geometry

Boundary conditions play an important role in buoyancy-driven flows. We employ the following set of boundary conditions for the velocity field:

1. Periodic: Imagine that the systems of Figs. 1.1 and1.3 embedded in a larger box. For such cases, we can employ periodic bound condition with

$$\mathbf{u}(\mathbf{x} + lL_x\hat{x} + mL_y\hat{y} + nL_z\hat{z}) = \mathbf{u}(\mathbf{x}), \tag{1.68}$$

   where l, m, n are integers, and the box is of the size $L_x \times L_y \times L_z$.

2. Often, a fluid is confined in box with top, bottom, and side walls. A generic boundary condition employed is no-slip, which is

$$\mathbf{u} = 0 \tag{1.69}$$

   at all the walls. Sometimes, for convenience of computation, no-slip boundary conditions are employed at the top and bottom walls but periodic boundary condition at the side walls.

3. When a fluid under consideration is over another fluid, for example air over water. In such cases, we employ free-slip boundary condition, which is

$$\mathbf{u}_\perp = 0; \quad \frac{\partial \mathbf{u}_\parallel}{\partial n} = 0 \tag{1.70}$$

   where $\mathbf{u}_\perp, \mathbf{u}_\parallel$ are respectively the velocity components perpendicular and parallel to the concerned surface, and n is the coordinate perpendicular to the wall. Note that $\mathbf{u} = \mathbf{u}_\perp + \mathbf{u}_\parallel$. For example, for an horizontal wall perpendicular to the z axis,

$$u_z = 0; \quad \frac{\partial u_x}{\partial z} = \frac{\partial u_y}{\partial z} = 0 \tag{1.71}$$

   We will show later that free-slip boundary condition is easier to implement in computer simulations.

The boundary conditions for the temperature or density are similar. Here we describe the boundary conditions for the temperature field.

1. Periodic: The temperature fluctuations are periodic along all the three directions:

$$\theta(\mathbf{x} + lL_x\hat{x} + mL_y\hat{y} + nL_z\hat{z}) = \theta(\mathbf{x}) \tag{1.72}$$

   where l, m, n are integers, and the box is of the size $L_x \times L_y \times L_z$.

2. Conducting : A constant temperature field at the walls:

$$\theta = 0 \tag{1.73}$$

3. Insulating: The heat flux at the wall, $K\nabla\theta$, is zero. To illustrate, for a vertical surface perpendicular to the x axis, the boundary condition on θ is

$$\frac{\partial\theta}{\partial x} = 0 \tag{1.74}$$

The other important factors that affect the flow properties are the box geometry and its size. The relative size is quantified using *aspect ratio*, which is the ratio of the box width and the box hight. We will show in this book that turbulent properties of the flow are somewhat independent of the box geometry. For example, turbulent thermal convection exhibits Kolmogorov's spectrum independent of the box geometry. However, large-scale structures of the flow are affected by the box geometry. For example, the rolls in a cylinder can freely rotate azimuthally, which is not the case in a cube.

Chapter 2

Fourier space description

Fourier decomposition of the flow field helps us quantify structures at different scales. In this chapter, we will discuss how to decompose the velocity and temperature fields of buoyancy-drive flows in Fourier space. First, we describe the RBC equations in Fourier space, and then tale up the equations for stably-stratified flows.

As described in Sec. 1.7, we impose periodic, free-slip, or no-slip boundary condition for RBC or stably-stratified flows. Periodic boundary condition is useful when the system under consideration is embedded inside a larger box. We employ free-slip and no-slip boundary conditions to describe flows confined within walls.

2.0.1 Definitions

Fourier basis is suitable to describe flows in a periodic box, say of size $L_x \times L_y \times L_z$. For RBC, the velocity and temperature fields are decomposed in Fourier basis as follows:

$$\mathbf{u}(\mathbf{r},t) = \sum_n \mathbf{u}(\mathbf{k},t)\exp(i\mathbf{k}\cdot\mathbf{r}), \tag{2.1}$$

$$\theta(\mathbf{r},t) = \sum_n \theta(\mathbf{k},t)\exp(i\mathbf{k}\cdot\mathbf{r}), \tag{2.2}$$

where $\mathbf{r}$ is the real space coordinate, $\mathbf{k} = (k_x, k_y, k_z)$ is the wavenumber with

$$k_x = \frac{2l\pi}{L_x};\quad k_y = \frac{2m\pi}{L_y};\quad k_z = \frac{2n\pi}{L_z}. \tag{2.3}$$

Here l, m, n are integers. The variables $\mathbf{u}(\mathbf{k},t)$ and $\theta(\mathbf{k},t)$ represent the Fourier amplitudes of velocity and temperature fields with wavenumber $\mathbf{k}$.

The inverse transform of the above is

$$\mathbf{u}(\mathbf{k},t) = \frac{1}{L_xL_yL_z}\int d\mathbf{r}\mathbf{u}(\mathbf{r},t)\exp(-i\mathbf{k}\cdot\mathbf{r}), \tag{2.4}$$

$$\theta(\mathbf{k},t) = \frac{1}{L_x L_y L_z}\int d\mathbf{r}\theta(\mathbf{r},t)\exp(-i\mathbf{k}\cdot\mathbf{r}), \tag{2.5}$$

where the aforementioned integral is performed over the whole box. It is easy to show that the Fourier transform of the product of two real functions f and g is a convolution:

$$(fg)(\mathbf{k}) = \sum_{\mathbf{p}} f(\mathbf{k}-\mathbf{p})g(\mathbf{p}) \tag{2.6}$$

and the Fourier transform of the derivative of a real function is given by

$$(df/dx_j)(\mathbf{k}) = ik_j f(\mathbf{k}) \tag{2.7}$$

Using the above identities, we can derive equations for RBC in Fourier space. For convenience we set $\rho_m = 1$. The equations

$$\frac{d}{dt}\mathbf{u}(\mathbf{k}) + \mathbf{N}_u(\mathbf{k}) = -i\mathbf{k}\sigma(\mathbf{k}) + \alpha g\theta(\mathbf{k})\hat{z} - \nu k^2\mathbf{u}(\mathbf{k}) \tag{2.8}$$

$$\frac{d}{dt}\theta(\mathbf{k}) + N_\theta(\mathbf{k}) = -\frac{d\bar{T}}{dz}u_z(\mathbf{k}) - \kappa k^2\theta(\mathbf{k}) \tag{2.9}$$

$$\mathbf{k}\cdot\mathbf{u}(\mathbf{k}) = 0, \tag{2.10}$$

where the nonlinear terms are given by

$$\mathbf{N}_u(\mathbf{k}) = i\sum_{\mathbf{p}}[\mathbf{k}\cdot\mathbf{u}(\mathbf{k}-\mathbf{p})]\mathbf{u}(\mathbf{p}) \tag{2.11}$$

$$N_\theta(\mathbf{k}) = i\sum_{\mathbf{p}}[\mathbf{k}\cdot\mathbf{u}(\mathbf{k}-\mathbf{p})]\theta(\mathbf{p}) \tag{2.12}$$

The equation for the pressure $\sigma(\mathbf{k})$ is derived by taking dot product of Eq. (2.8) with $\mathbf{k}$, and employing $\mathbf{k}\cdot\mathbf{u}(\mathbf{k}) = \mathbf{0}$ that yields

$$\sigma(\mathbf{k}) = \frac{1}{k^2}[i\mathbf{k}\cdot\mathbf{N}(\mathbf{k}) - i\alpha g k_z\theta(\mathbf{k})] \tag{2.13}$$

The above equations can be written in tensorial form as

$$\frac{d}{dt}u_i(\mathbf{k}) = -ik_i\sigma(\mathbf{k}) - ik_j\sum_{\mathbf{p}}u_j(\mathbf{k}-\mathbf{p})u_i(\mathbf{p}) + \alpha g\theta(\mathbf{k})\delta_{i,3} - \nu k^2 u_i(\mathbf{k}), \tag{2.14}$$

$$\frac{d}{dt}\theta(\mathbf{k}) = -\frac{d\bar{T}}{dz}u_z(\mathbf{k}) - ik_j\sum_{\mathbf{p}}u_j(\mathbf{k}-\mathbf{p})\theta(\mathbf{p}) - \kappa k^2\theta(\mathbf{k}), \tag{2.15}$$

$$k_i u_i(\mathbf{k}) = 0. \tag{2.16}$$

In Eq. (2.14), i represents two things: $\sqrt{-1}$ in front of the $k_i\sigma(\mathbf{k})$ term and $i = 1,2,3$ in u_i. Note that $i = 1,2,3$ represents x, y, z components respectively.

One of the nondimensionalized version of RBC equations is

$$\frac{d}{dt}\mathbf{u}(\mathbf{k}) + \mathbf{N}_u(\mathbf{k}) = -i\mathbf{k}\sigma(\mathbf{k}) + \mathrm{RaPr}\theta(\mathbf{k})\hat{z} - \mathrm{Pr}k^2\mathbf{u}(\mathbf{k}) \tag{2.17}$$

$$\frac{d}{dt}\theta(\mathbf{k}) + N_\theta(\mathbf{k}) = u_z(\mathbf{k}) - \kappa k^2\theta(\mathbf{k}) \tag{2.18}$$

$$\mathbf{k}\cdot\mathbf{u}(\mathbf{k}) = 0, \tag{2.19}$$

The corresponding equations for the stably-stratified flows are

$$\frac{d}{dt}\mathbf{u}(\mathbf{k}) + \mathbf{N}_u(\mathbf{k}) = -i\mathbf{k}\sigma(\mathbf{k}) - Nb(\mathbf{k})\hat{z} - \nu k^2\mathbf{u}(\mathbf{k}) \tag{2.20}$$

$$\frac{d}{dt}b(\mathbf{k}) + N_b(\mathbf{k}) = Nu_z(\mathbf{k}) - \kappa k^2\theta(\mathbf{k}) \tag{2.21}$$

$$\mathbf{k}\cdot\mathbf{u}(\mathbf{k}) = 0, \tag{2.22}$$

where N is the Brunt-Väisälä frequency, and the nonlinear terms are given by

$$\mathbf{N}_u(\mathbf{k}) = i\sum_{\mathbf{p}}[\mathbf{k}\cdot\mathbf{u}(\mathbf{k}-\mathbf{p})]\mathbf{u}(\mathbf{p}), \tag{2.23}$$

$$N_b(\mathbf{k}) = i\sum_{\mathbf{p}}[\mathbf{k}\cdot\mathbf{u}(\mathbf{k}-\mathbf{p})]b(\mathbf{p}). \tag{2.24}$$

Pressure $\sigma(\mathbf{k})$ is computed using

$$\sigma(\mathbf{k}) = \frac{1}{k^2}[i\mathbf{k}\cdot\mathbf{N}(\mathbf{k}) + iNk_z\theta(\mathbf{k})]. \tag{2.25}$$

2.0.2 Energy and entropy

The energy of a velocity Fourier mode, called modal energy energy, is given by

$$E_u(\mathbf{k}) = \frac{1}{2}|\mathbf{u}(\mathbf{k})|^2. \tag{2.26}$$

Using Eq. (2.2) and the orthogonality relation, we can show that the average kinetic energy in the box is

$$\frac{1}{L_xL_yL_z}\int d\mathbf{r}\frac{1}{2}|\mathbf{u}(\mathbf{r})|^2 = \sum_{\mathbf{k}}\frac{1}{2}|\mathbf{u}(\mathbf{k})|^2. \tag{2.27}$$

This is *Parseval's theorem.* Similarly modal entropy spectrum, $E_\theta(\mathbf{k})$, is defined as

$$E_\theta(\mathbf{k}) = \frac{1}{2}|\theta(\mathbf{k}')|^2. \tag{2.28}$$

Note that the above definition of entropy differs from the thermodynamic entropy.

To derive a dynamical equation for $|\mathbf{u}(\mathbf{k})|^2/2$, we multiply Eq. (2.14) with $u_i^*(\mathbf{k})$ and sum over i that yields

$$\begin{aligned} u_i^*(\mathbf{k})\frac{d}{dt}u_i(\mathbf{k}) &= -ik_i u_i^*(\mathbf{k})\sigma(\mathbf{k}) - ik_j\sum_{\mathbf{p}} u_j(\mathbf{k}-\mathbf{p})u_i(\mathbf{p})u_i^*(\mathbf{k}) \\ &\quad +\alpha g\theta(\mathbf{k})u_z^*(\mathbf{k}) - \nu k^2|\mathbf{u}(\mathbf{k})|^2 \end{aligned} \tag{2.29}$$

Note that $-ik_i u_i^*(\mathbf{k})\sigma(\mathbf{k}) = 0$ due to the incompressibility condition, $\mathbf{k}\cdot\mathbf{u}(\mathbf{k}) = 0$. Hence, the pressure does not contribute to the energy transfers. Now we add the above equation with its complex conjugate that yields

$$\begin{aligned} \frac{d}{dt}E_u(\mathbf{k}) &= \Im\left[\sum_{\mathbf{p}}\left[\mathbf{k}\cdot\mathbf{u}(\mathbf{q})\right]\left[\mathbf{u}(\mathbf{p})\cdot\mathbf{u}^*(\mathbf{k})\right]\right] + \alpha g\Re[\theta(\mathbf{k})u_z^*(\mathbf{k})] \\ &\quad -2\nu k^2 E_u(\mathbf{k}), \end{aligned} \tag{2.30}$$

where $\mathbf{q} = \mathbf{k} - \mathbf{p}$, and $\Re, \Im$ stand respectively for the real and imaginary parts of the argument. In the above equation, the rate of change of $E_u(\mathbf{k})$ occurs due to (a) the nonlinear energy transfers from modes, quantified by the first term of right hand side, (b) buoyancy $\alpha g\Re[\theta(\mathbf{k})u_z^*(\mathbf{k})]$, and (c) the dissipation term $-2\nu k^2 E_u(\mathbf{k})$. Following a similar procedure, we can derive an equation for the entropy spectrum:

$$\begin{aligned} \frac{d}{dt}E_\theta(\mathbf{k}) &= \Im\left[\sum_{\mathbf{p}}\left[\mathbf{k}\cdot\mathbf{u}(\mathbf{q})\right]\left[\theta(\mathbf{p})\theta^*(\mathbf{k})\right]\right] - \frac{d\bar{T}}{dz}\Re[\theta(\mathbf{k})u_z^*(\mathbf{k})] \\ &\quad -2\kappa k^2 E_\theta(\mathbf{k}), \end{aligned} \tag{2.31}$$

For stably-stratified flows, we define modal spectra for the density field and potential energy $b^2/2$ as

$$E_\rho(\mathbf{k}) = \frac{1}{2}|\rho(\mathbf{k}')|^2, \tag{2.32}$$

$$E_b(\mathbf{k}) = \frac{1}{2}|b(\mathbf{k}')|^2. \tag{2.33}$$

The dynamical equations for $E_\rho(\mathbf{k})$ and $E_b(\mathbf{k})$ are

$$\begin{aligned} \frac{d}{dt}E_u(\mathbf{k}) &= \Im\left[\sum_{\mathbf{p}}\left[\mathbf{k}\cdot\mathbf{u}(\mathbf{q})\right]\left[\mathbf{u}(\mathbf{p})\cdot\mathbf{u}^*(\mathbf{k})\right]\right] + N\Re[b(\mathbf{k})u_z^*(\mathbf{k})] \\ &\quad -2\nu k^2 E_u(\mathbf{k}), \end{aligned} \tag{2.34}$$

$$\begin{aligned} \frac{d}{dt}E_b(\mathbf{k}) &= \Im\left[\sum_{\mathbf{p}}\left[\mathbf{k}\cdot\mathbf{u}(\mathbf{q})\right]\left[b(\mathbf{p})b^*(\mathbf{k})\right]\right] - N\Re[b(\mathbf{k})u_z^*(\mathbf{k})] \\ &\quad -2\kappa k^2 E_b(\mathbf{k}) \end{aligned} \tag{2.35}$$

For homogenous and isotropic turbulence, the energy and entropy of all the modes in a shell are statistically same. Hence, it is customary to define one-dimensional spectrum, $E_u(k), E_\theta(k), E_\rho(k)$ and $E_b(k)$, which are sums of all the modes of a shell of unit radius [1]

$$E_u(k) = \sum_{k-1<k'\leq k} \frac{1}{2}|\mathbf{u}(\mathbf{k})|^2, \tag{2.37}$$

$$E_\theta(k) = \sum_{k-1<k'\leq k} \frac{1}{2}|\theta(\mathbf{k})|^2, \tag{2.38}$$

$$E_\rho(k) = \sum_{k-1<k'\leq k} \frac{1}{2}|\rho(\mathbf{k})|^2, \tag{2.39}$$

$$E_b(k) = \sum_{k-1<k'\leq k} \frac{1}{2}|b(\mathbf{k})|^2. \tag{2.40}$$

The dynamical equations for the above quantities can be obtained by summing equations over all the $\mathbf{k}$ modes. For example, equations for $E_u(k)$ is

$$\begin{aligned}\frac{d}{dt}E_u(k) = & \sum_{k-1<k'\leq k} \Im\left[\sum_{\mathbf{p}} [\mathbf{k}\cdot\mathbf{u}(\mathbf{q})]\,[\mathbf{u}(\mathbf{p})\cdot\mathbf{u}^*(\mathbf{k})]\right] + \sum_{k-1<k'\leq k} \alpha g \Re[\theta(\mathbf{k})u_z^*(\mathbf{k})] \\ & - \sum_{k-1<k'\leq k} 2\nu k^2 E_u(\mathbf{k})\end{aligned} \tag{2.41}$$

2.1 Reality condition

The velocity, density, and temperature fields are real. Hence

$$\mathbf{u}^*(-\mathbf{k},t) = \frac{1}{L_x L_y L_z}\int d\mathbf{r}\mathbf{u}(\mathbf{r},t)\exp(-i\mathbf{k}\cdot\mathbf{r}) \tag{2.42}$$

$$= \mathbf{u}^*(\mathbf{k},t). \tag{2.43}$$

We illustrate this in Fig. 2.44. Similarly for the temperature field

$$\theta(-\mathbf{k},t) = \theta^*(\mathbf{k},t). \tag{2.44}$$

Due to the above relation, we need to store only half the modes that helps us in numerical simulations.

[1] For continuum k, $E_X(k)$, where $X = u, \theta$ or b, is defined as

$$\int_k^{k+dk} E_X(k')dk' \approx E_X(k')dk', \tag{2.36}$$

where the sum is performed over all the modes in a the shell whose inner and outer radii are k and $k+dk$ respectively. Note that $\int E_X(k')dk' = E_X$.

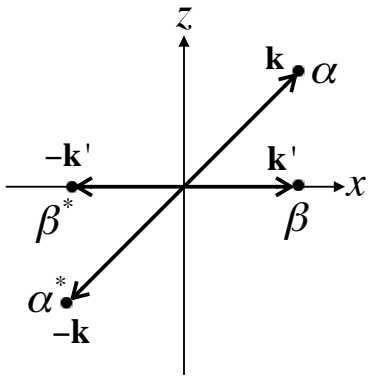

Figure 2.1: reality condition

2.2 Free-slip basis functions for RBC

Thermal convection typically involves walls or boundaries, hence $\exp(i\mathbf{k}\cdot\mathbf{r})$ are not appropriate basis functions for the same. Typical boundary condition for RBC are either free-slip or no-slip. We describe appropriate basis functions for such boundary conditions.

The free-slip boundary condition is

$$\mathbf{u}_\perp = 0; \quad \frac{\partial \mathbf{u}_\parallel}{\partial n} = 0, \tag{2.45}$$

where $u_\perp$ and $u_\parallel$ are respectively the velocity components normal and parallel to the surface, and n is the coordinate parallel to the wall. Let us assume that the fluid is confined in a cube of size $(\pi \times \pi \times \pi)$ with free-slip boundary condition applicable on all the walls. For such flows, the basis functions for the three components of the velocities are

$$\begin{aligned}
u_x &= \hat{u}_x(k_x,k_y,k_z)(2\sin k_x x)(\delta_{k_y,0}+2\cos k_y y)(\delta_{k_z,0}+2\cos k_z z) && (2.46)\\
u_y &= \hat{u}_y(k_x,k_y,k_z)(\delta_{k_x,0}+2\cos k_x x)(2\sin k_y y)(\delta_{k_z,0}+2\cos k_z z) && (2.47)\\
u_z &= \hat{u}_z(k_x,k_y,k_z)(\delta_{k_x,0}+2\cos k_x x)(\delta_{k_y,0}+2\cos k_y y)(2\sin k_z z). && (2.48)
\end{aligned}$$

We term the above as *free-slip basis functions*, with the hat representing the amplitudes of free-slip basis function. Note that k_x, k_y, k_z are positive integers (including zero), unlike Fourier wavenumbers that range from $-\infty$ to ∞.

For the temperature field, either conducting or insulating boundary conditions are used. The conducting boundary condition is

$$T = \text{const}; \quad \text{or} \quad \theta = 0, \tag{2.49}$$

while the insulating boundary condition is

$$\frac{\partial T}{\partial n} = \frac{\partial \theta}{\partial n} = 0. \tag{2.50}$$

The following function

$$\theta \quad = \quad \hat{\theta}(k_x, k_y, k_z)(\delta_{k_x,0} + 2\cos k_x x)(\delta_{k_y,0} + 2\cos k_y y)(2\sin k_z z). \quad (2.51)$$

is suitable for conducting walls at $z = 0, \pi$, and insulating walls at the side walls at $x = 0, \pi$, and $y = 0, \pi$.

The Fourier basis function, which is suitable for a periodic box, is $\exp[i(k_x x + k_y y + k_z z)]$, where k_x, k_y, k_z take both positive and negative values. We can convert the coefficient of a free-slip basis function to the corresponding Fourier basis function using $2\cos x = [\exp(ix) + \exp(-ix)]$ and $2\sin x = [\exp(ix) - \exp(-ix)]/i$. In Table **??**, we list the Fourier amplitudes corresponding to the amplitude $\hat{\mathbf{u}}(k_x, k_y, k_z)$ for the free-slip basis. As an example,

$$\begin{aligned} u_x &= \hat{u}_x(1,0,1)(2\sin x)(2\cos z) \\ &= \hat{u}_x(1,0,1)\frac{1}{i}(\exp(x) - \exp(-x))(\exp(z) + \exp(-z)) \\ &= \hat{u}_x(1,0,1)[\frac{1}{i}\exp(x+z)\frac{1}{i}\exp(x-z) \\ &\quad -\frac{1}{i}\exp(-x+z) - \frac{1}{i}\exp(-x-z)] \end{aligned} \quad (2.52)$$

Therefore,

$$u_x(1,0,1) = u_x(1,0,-1) = \frac{1}{i}\hat{u}_x(1,0,1) \quad (2.53)$$

$$u_x(-1,0,1) = u_x(-1,0,-1) = -\frac{1}{i}\hat{u}_x(1,0,1) \quad (2.54)$$

as shown in Table 2.1.

Table 2.1: Transformation rules from the free-slip amplitudes $\hat{u}_x(k_x, k_y, k_z)$ to the Fourier amplitudes.

mode	u_x	u_y	u_z
(k_x, k_y, k_z)	$\frac{1}{i}\hat{u}_x(k_x, k_y, k_z)$	$\frac{1}{i}\hat{u}_y(k_x, k_y, k_z)$	$\frac{1}{i}\hat{u}_z(k_x, k_y, k_z)$
$(k_x, k_y, -k_z)$	$\frac{1}{i}\hat{u}_x(k_x, k_y, k_z)$	$\frac{1}{i}\hat{u}_y(k_x, k_y, k_z)$	$-\frac{1}{i}\hat{u}_z(k_x, k_y, k_z)$
$(k_x, -k_y, k_z)$	$\frac{1}{i}\hat{u}_x(k_x, k_y, k_z)$	$-\frac{1}{i}\hat{u}_y(k_x, k_y, k_z)$	$\frac{1}{i}\hat{u}_z(k_x, k_y, k_z)$
$(k_x, -k_y, -k_z)$	$\frac{1}{i}\hat{u}_x(k_x, k_y, k_z)$	$-\frac{1}{i}\hat{u}_y(k_x, k_y, k_z)$	$-\frac{1}{i}\hat{u}_z(k_x, k_y, k_z)$
$(-k_x, k_y, k_z)$	$-\frac{1}{i}\hat{u}_x(k_x, k_y, k_z)$	$\frac{1}{i}\hat{u}_y(k_x, k_y, k_z)$	$\frac{1}{i}\hat{u}_z(k_x, k_y, k_z)$
$(-k_x, k_y, -k_z)$	$-\frac{1}{i}\hat{u}_x(k_x, k_y, k_z)$	$\frac{1}{i}\hat{u}_y(k_x, k_y, k_z)$	$-\frac{1}{i}\hat{u}_z(k_x, k_y, k_z)$
$(-k_x, -k_y, k_z)$	$-\frac{1}{i}\hat{u}_x(k_x, k_y, k_z)$	$-\frac{1}{i}\hat{u}_y(k_x, k_y, k_z)$	$\frac{1}{i}\hat{u}_z(k_x, k_y, k_z)$
$(-k_x, -k_y, -k_z)$	$-\frac{1}{i}\hat{u}_x(k_x, k_y, k_z)$	$-\frac{1}{i}\hat{u}_y(k_x, k_y, k_z)$	$-\frac{1}{i}\hat{u}_z(k_x, k_y, k_z)$

Example: Construct 2D incompressible velocity field in xz plane whose $u_x = 4A\sin k_x z \cos k_z z$.

Solution: When we compare the expression $u_x = 4A \sin k_x z \cos k_z z$ with Eq. (2.46), we obtain $\hat{u}_x(k_x, 0, k_z) = A$. The incompressible condition $\mathbf{k} \cdot \hat{\mathbf{u}}(\mathbf{k}) = 0$ yields

$$\hat{u}_z(k_x, 0, k_z) = -\frac{k_x}{k_z} \hat{u}_x(k_x, 0, k_z) = -\frac{k_x}{k_z} A. \tag{2.55}$$

Therefore, the velocity field is

$$\mathbf{u} = \hat{x} 4A \sin k_x x \cos k_z z - \hat{z} \frac{k_x}{k_z} 4A \cos k_x x \sin k_z z. \tag{2.56}$$

The above form of velocity is however valid when both k_x and k_y are nonzero. For modes with $k_z = 0$,

$$\mathbf{u} = \hat{z} 2A \cos k_x x, \tag{2.57}$$

while for $k_x = 0$,

$$\mathbf{u} = \hat{x} 2B \cos k_z z. \tag{2.58}$$

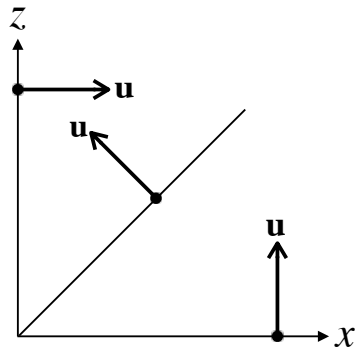

Figure 2.2: Example 1

2.3 no-slip boundary condition for RBC

A realistic boundary condition for fluid flows is the no-slip boundary condition, which is $\mathbf{u} = 0$ at the surface. Unfortunately, Fourier expansion is not suitable for this boundary condition, and more complex expansion called Chebyshev polynomials are employed for this purpose. The discussion on Chebyshev is beyond the scope of this book; the reader is referred to Canuto *et al.* [**?**] XXX.

Typically, flows with no-slip boundary conditions are simulated using finite-difference, finite-volume, finite-element, or spectral-element methods in real space. The mesh is refined appropriately to take care of the steep variations of the velocity and temperature fields.

The no-slip boundary condition picks the viscous boundary layer. For turbulent flows with moderate Prandtl numbers, the viscous boundary layer is quite

thin. Hence, the structures within the boundary layers are of very small size compared to the box size. Hence, the modal spectra of such modes would contribute to large-wavenumber regime of $E(k)$, and it is expected not to affect the inertial range properties. Therefore, free-slip basis could be employed to study energy spectrum and related quantities.

The energy transfers among the interacting Fourier modes provide valuable diagnostics for understanding patterns, chaos, and turbulence in buoyancy-driven flows. We will show later that the energy flux provides valuable information on the dynamics. These computations are conveniently performed using the Fourier basis functions [**?**]. Note however that Fourier transformation is typically performed on data sampled at uniform mesh. Typical output of finite-difference, finite-volume, finite-element, or spectral-element computations are on nonuniform mesh, which are interpolated to uniform mesh for spectral analysis. Chandra and Verma [**?**, **?**] performed such computations for computation of dominant Fourier modes in 2D RBC.

Chapter 3

Waves in stably stratified flows

Stably stratified flows are linearly stable hence they support waves under linear perturbation. In this chapter we derive wave solution for Stably stratified flows. These waves are called *internal gravity waves* because they occur inside the bulk.

We start with Eqs. (2.20-2.22). Under linear limit, and for $\nu = \kappa = 0$, the above equations reduce to

$$\begin{aligned} \frac{d}{dt}\mathbf{u}(\mathbf{k}) &= -i\mathbf{k}\frac{\sigma(\mathbf{k})}{\rho_m} - Nb(\mathbf{k})\hat{z}, && (3.1)\\ \frac{d}{dt}b(\mathbf{k}) &= N\hat{u}_z(\mathbf{k}), && (3.2)\\ \mathbf{k}\cdot\mathbf{u}(\mathbf{k}) &= 0, && (3.3) \end{aligned}$$

where N is the *Brunt-Väisälä frequency*

$$N = \sqrt{\frac{g}{\rho_m}\left|\frac{d\bar{\rho}}{dz}\right|}, \tag{3.4}$$

and b is the following form of normalised density in the units of velocity:

$$b = \frac{g}{N}\frac{\rho}{\rho_m}, \tag{3.5}$$

We compute the pressure $\sigma(\mathbf{k})$ by taking dot product with $\mathbf{k}$ to Eq. (3.1), and employing $\mathbf{k}\cdot\mathbf{u}(\mathbf{k}) = 0$. As a result we obtain

$$\sigma(\mathbf{k}) = iN\rho_m\frac{k_z}{k^2}b(\mathbf{k}) \tag{3.6}$$

that yields

$$\frac{d}{dt}u_z(\mathbf{k}) = -\frac{k_\perp^2}{k^2}Nb(\mathbf{k}), \tag{3.7}$$

In matrix form, Eqs. (3.3-3.7) appear as

$$\frac{d}{dt}\left(u_z(\mathbf{k})b(\mathbf{k})\right) = \left(0 - \frac{k_\perp^2}{k^2}NN0\right)\left(u_z(\mathbf{k})b(\mathbf{k})\right) = A\left(u_z(\mathbf{k})b(\mathbf{k})\right) \tag{3.8}$$

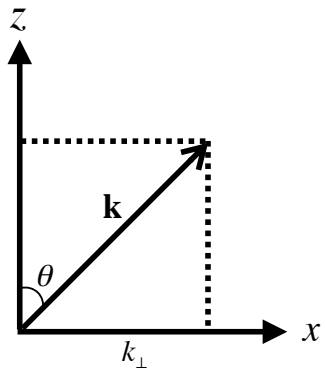

Figure 3.1: density...

The eigenvalues of the matrix A are $\lambda_\pm = \pm\omega$ with

$$\omega = N\frac{k_\perp}{k} = N\sin\zeta, \tag{3.9}$$

where ζ is the angle between $\mathbf{k}$ and $\hat{z}$ (see Fig. 3.1 for an illustration). The corresponding eigenvectors are

$$\left(1 - \frac{ik}{k_\perp}\right); \quad \left(1\frac{ik}{k_\perp}\right). \tag{3.10}$$

The solution for λ_+ is

$$u_z(\mathbf{k},t) = A_+\exp(i\omega t) \tag{3.11}$$

$$b(\mathbf{k},t) = -i\frac{kA_+}{k_\perp}\exp(i\omega t) \tag{3.12}$$

where $A_+ = |A_+|\exp(i\phi_+)$, a complex number, is the amplitude. By transforming the above to real space, we obtain

$$\begin{aligned} u_z(\mathbf{r},t) &= A_+\exp(i\mathbf{k}\cdot\mathbf{r} + i\omega t) + c.c. \\ &= |A_+|\cos(\mathbf{k}\cdot\mathbf{r} + \omega t + \phi_+), \end{aligned} \tag{3.13}$$

$$\begin{aligned} b(\mathbf{r},t) &= -\frac{ikA_+}{k_\perp}\exp(i\mathbf{k}\cdot\mathbf{r} + i\omega t) + c.c. \\ &= |A_+|\frac{k}{k_\perp}\sin(\mathbf{k}\cdot\mathbf{r} + \omega t + \phi_+). \end{aligned} \tag{3.14}$$

The above solution corresponds to internal gravity waves moving in the direction of $-\mathbf{k}$. By following a similar procedure we obtain the solution corresponding to λ_- as

$$\begin{aligned} u_z(\mathbf{r},t) &= A_- \exp(i\mathbf{k}\cdot\mathbf{r} - i\omega t) + c.c. \\ &= |A_-| \cos(\mathbf{k}\cdot\mathbf{r} - \omega t + \phi_-), \qquad (3.15) \\ b(\mathbf{r},t) &= \frac{ikA_-}{k_\perp} \exp(i\mathbf{k}\cdot\mathbf{r} - i\omega t) + c.c. \\ &= -|A_-| \frac{k}{k_\perp} \sin(\mathbf{k}\cdot\mathbf{r} - \omega t + \phi_-). \qquad (3.16) \end{aligned}$$

Here $A_- = |A_-| \exp(i\phi_-)$. The above solution represents internal gravity waves moving along $\mathbf{k}$. For 2D waves with $\mathbf{k} = k_x\hat{x} + k_z\hat{z}$, incompressiblity condition yields

$$u_x = -\frac{k_z}{k_x} u_z \qquad (3.17)$$

We illustrate the internal gravity waves moving along $\mathbf{k}$ using three limiting cases:

1. For $\mathbf{k} = k_x\hat{x}$, Fig. 3.1(a) illustrates a wave moving along $\hat{x}$:

   $$\mathbf{u}(\mathbf{r},t) = A_- \cos(k_x x - \omega t)\hat{z} \qquad (3.18)$$

   For this wave, $k_\perp = k_x = k$ or $\zeta = \pi/2$. Therefore, $\omega = N$ and $u_x = 0$ (see Eq. (3.17)). We illustrate the above wave propagation in Fig. 3.2(a). Note that the fluid parcels are oscillating up and down vertically due to gravity.

2. For $\mathbf{k} = k_z\hat{z}$,

   $$\mathbf{u}(\mathbf{r},t) = A\cos(k_z z)\hat{x}. \qquad (3.19)$$

   Here $\omega = 0$, $u_z = 0$, and there is no gravity wave. See Fig. 3.2(b) for an illustration. Note that $u_z = 0$. See Fig. 3.1(b) for an illustration. The velocity vectors of Fig. 3.2(b) provide shear to the flow, and they are not connected to gravitational oscillations.

3. For $\mathbf{k} = k_x\hat{x} + k_z\hat{z}$,

   $$\mathbf{u}(\mathbf{r},t) = A_- \cos(k_x x + k_z z - \omega t)\hat{n}. \qquad (3.20)$$

   where $\omega = Nk_x/k = N\sin b$ with $k = \sqrt{k_x^2 + k_y^2}$, and $\mathbf{u}$ is perpendicular to $\mathbf{k}$ as shown in the figure. See Fig. 3.2(c) for an illustration. Note that both u_x and u_z have the same frequency ω. As described in items (1,2), for $\mathbf{k} = k_x\hat{x}$, u_z oscillates with the frequency of ω. But $\omega = 0$ for $\mathbf{k} = k_z\hat{z}$. For a combination, $\mathbf{k} = k_x\hat{x} + k_z\hat{z}$, the oscillation frequency takes an intermediate value due to the inertia of u_x, which is made to oscillate with the same frequency as u_z.

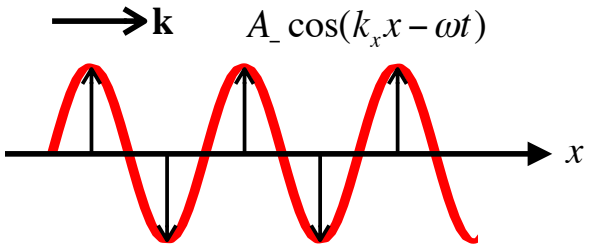

(a)

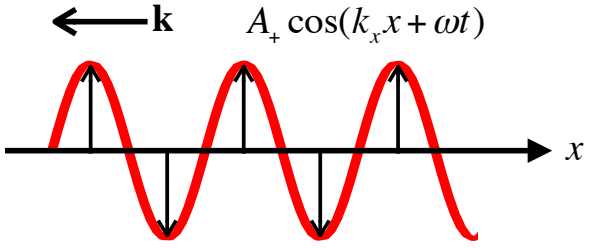

(b)

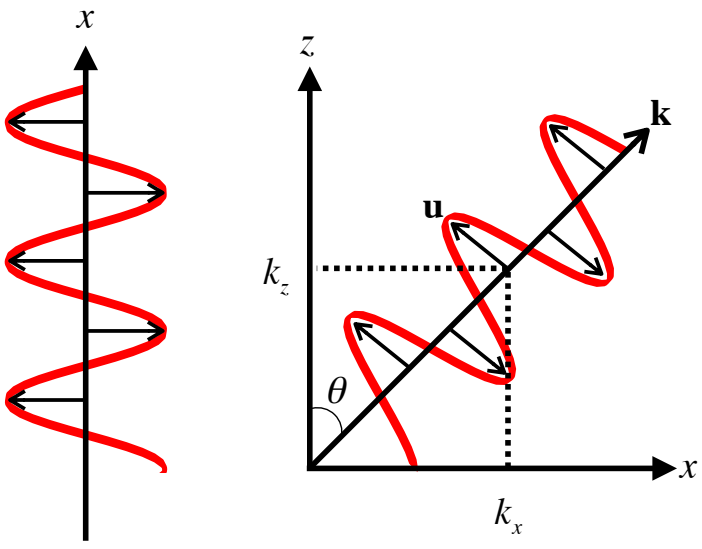

(c) (d)

Figure 3.2: density...

A general solution is combination of the above solutions, i.e.,

$$u_z(\mathbf{r},t) = |A_+|\cos(\mathbf{k}\cdot\mathbf{r}+\omega t+\phi_+) + |A_-|\cos(\mathbf{k}\cdot\mathbf{r}-\omega t+\phi_-) \quad (3.21)$$

$$b(\mathbf{r},t) = \frac{k}{k_\perp}\left[|A_+|\sin(\mathbf{k}\cdot\mathbf{r}+\omega t+\phi_+) - |A_-|\cos(\mathbf{k}\cdot\mathbf{r}-\omega t+\phi_-)\right] \quad (3.22)$$

which is a superposition of waves travelling parallel and antiparallel to $\mathbf{k}$.

Another important wave driven by buoyancy is surface gravity wave, which will be discussed in the next chapter.

Chapter 4

Instability in thermal convection

When a fluid confined between two plates is subjected to an adverse temperature gradient, as shown in Fig. 1.3(c), the flow exhibits instability for temperature profiles beyond a critical temperature gradient. In this chapter we derive instability criteria for RBC. We will also discuss the properties of the solution.

In this chapter, we solve the linearised version of RBC equations. For the same we drop the nonlinear terms of Eqs. (1.17-1.19) that yields the following linearised equations for u_z and θ

$$\begin{aligned} \frac{\partial}{\partial t}\mathbf{u} &= -\nabla\sigma + \mathrm{RaPr}\theta\hat{z} + \mathrm{Pr}\nabla^2\mathbf{u}, & (4.1)\\ \frac{\partial\theta}{\partial t} &= u_z + \nabla^2\theta. & (4.2)\\ \nabla\cdot\mathbf{u} &= 0. & (4.3) \end{aligned}$$

It is quite convenient to use work out the instability condition using the equation for u_z:

$$\frac{\partial u_z}{\partial t} = -\partial_z\sigma + \mathrm{RaPr}\theta + \mathrm{Pr}\nabla^2 u_z, \tag{4.4}$$

The u_x component is determined using the incompressibility condition, Eq. (4.3).

First we solve the above equations for the free-slip boundary condition.

4.1 RBC instability for Free-slip boundary condition

We consider two infinite horizontal plates at $z = 0$ and $z = 1$. On the plates, we employ free-slip boundary condition for the velocity field and conducting boundary condition for the temperature. We apply periodic boundary condition

along the horizontal direction. The following basis functions satisfy the above boundary conditions:

$$\begin{aligned} u_z(x,z) &= u_z(\mathbf{k}) 2\sin(n\pi z)\exp(i\mathbf{k}_\perp\cdot\mathbf{r}_\perp) + c.c., && (4.5)\\ \theta(x,z) &= \theta_z(\mathbf{k}) 2\sin(n\pi z)\exp(i\mathbf{k}_\perp\cdot\mathbf{r}_\perp) + c.c., && (4.6)\end{aligned}$$

where n is integer, $\mathbf{k}_\perp = k_x\hat{x} + k_y\hat{y}$, and $\mathbf{r}_\perp = x\hat{x} + y\hat{y}$. Substitution of the above in Eqs. (4.4, 4.2) yields

$$\begin{aligned} \frac{d}{dt}u_z(\mathbf{k}) &= -i\mathbf{k}\sigma(\mathbf{k}) + \mathrm{RaPr}\theta(\mathbf{k}) - \mathrm{Pr}k^2 u_z(\mathbf{k}) && (4.7)\\ \frac{d}{dt}\theta(\mathbf{k}) &= u_z(\mathbf{k}) - k^2\theta(\mathbf{k}) && (4.8)\end{aligned}$$

We compute the pressure $\sigma(\mathbf{k})$ by taking dot product with $\mathbf{k}$ to Eq. (3.1), and employing $\mathbf{k}\cdot\mathbf{u}(\mathbf{k}) = 0$. As a result we obtain

$$\sigma(\mathbf{k}) = -i\frac{k_z}{k^2}\mathrm{RaPr}\theta(\mathbf{k}) \tag{4.9}$$

substitution of which in Eq. (4.10) yields

$$\frac{d}{dt}u_z(\mathbf{k}) = \mathrm{RaPr}\frac{k_\perp^2}{k^2}\theta(\mathbf{k}) - \mathrm{Pr}k^2 u_z(\mathbf{k}) \tag{4.10}$$

Equations (4.10, 4.8) in matrix form are

$$\frac{d}{dt}\left(u_z(\mathbf{k})\theta(\mathbf{k})\right) = \left(-\mathrm{Pr}k^2 \mathrm{RaPr}k_\perp^2/k^2 1 - k^2\right)\left(u_z(\mathbf{k})\theta(\mathbf{k})\right) = A\left(u_z(\mathbf{k})\theta(\mathbf{k})\right) \tag{4.11}$$

We solve the above equations using matrix method. The eigenvalues of the stability matrix A is

$$\lambda_\pm = \frac{1}{2}\left(\mathrm{Tr} \pm \sqrt{\mathrm{Tr}^2 - 4\mathrm{Det}}\right) \tag{4.12}$$

where $\mathrm{Tr} = -(\mathrm{Pr}+1)k^2$ is the trace of A, while $\mathrm{Det} = \mathrm{Pr}k^4 - \mathrm{RaPr}k_\perp^2/k^2$ is the determinant of A. The solution of the above equations is

$$\begin{aligned} \theta(\mathbf{k},t) &= a_1\exp(\lambda_+ t) + a_2\exp(\lambda_- t), && (4.13)\\ u_z(\mathbf{k},t) &= a_1(\lambda_+ + k^2)\exp(\lambda_+ t) + a_2(\lambda_- + k^2)\exp(\lambda_- t), && (4.14)\end{aligned}$$

where $k^2 = (n\pi)^2 + k_\perp^2$, and a_1, a_2 are constants that are determined using initial condition $[\theta(\mathbf{k},0), u_z(\mathbf{k},0)]$.

We can determine the properties of $\lambda_\pm$ using the properties of the matrix A. The eigenvalues $\lambda_\pm$ are always real since the argument of the square-root

$$\mathrm{Tr}^2 - 4\mathrm{Det} = (\mathrm{Pr}-1)^2 k^4 + 4\mathrm{RaPr}\frac{k_\perp^2}{k^2} \tag{4.15}$$

is real and positive-definite.

Note that Tr < 0. Therefore, when Det > 0, $\sqrt{\text{Tr}^2 - 4\text{Det}} < |\text{Tr}|$ that leads to $\lambda_\pm < 0$ and dying solution

$$u_z(\mathbf{k}, t), \theta(\mathbf{k}, t) \to 0 \tag{4.16}$$

This is the stable solution for which the heat is transported by conduction. However, for Det < 0, $\sqrt{\text{Tr}^2 - 4\text{Det}} > |\text{Tr}|$. Therefore, $\lambda_+ > 0$ and $\lambda_- < 0$, hence

$$u_z(\mathbf{k}, t), \theta(\mathbf{k}, t) \to \exp(\lambda_+ t). \tag{4.17}$$

grows with time asymptotically. The component with $\exp(\lambda_- t)$ goes to zero. This is the unstable solution of the linear equation.

The transition from decaying to growing solution occurs at $\lambda_+ = 0$ that happens when Det $= 0$ [see Eq. (4.12], or at

$$\text{Ra}_c = \frac{k^6}{k_\perp^2} = \frac{(k_\perp^2 + n^2\pi^2)^3}{k_\perp^2} \tag{4.18}$$

This condition is called *neutral stability*.

The critical number Ra_c depends on n and $k_\perp$, as shown in Fig. XXX for different n and $k_\perp$. For a given n, the minimum value of Ra_c occurs for $k_\perp = k_c$, where k_c is determined using

$$\partial_{k_\perp} \text{Ra}_c|_{k_c} = 0 \tag{4.19}$$

that yields

$$k_c = \frac{n\pi}{\sqrt{2}}, \tag{4.20}$$

$$k^2 = k_c^2 + (n\pi)^2 = 3n^2\pi^2/2 \tag{4.21}$$

substitution of which in Eq. (4.18) yields

$$\text{Ra}_{c,\min} = \frac{\left(\pi^2 + \pi^2/2\right)^3}{\pi^2/2} = \frac{27n^2\pi^4}{4}. \approx 657.511n^2 \tag{4.22}$$

The values of k_c and Ra_c are exhibited in Fig. 4.1. When we increase Ra (in experiment Δ), the first mode to become unstable is $n = 1$ with wavenumber $\mathbf{k} = (\pi/\sqrt{2})\hat{x} + \pi\hat{z}$. Higher modes get excited at larger Ra. Of course, nonlinear interactions, to be discussed in Chapter XXX, excite more modes.

Without loss of generality, we can choose $\mathbf{k}_\perp$ along $\hat{x}$. The incompressibility condition yields

$$u_x = -i\frac{k_z}{k_c} u_z, \tag{4.23}$$

The growing solution for $n = 1$ is

$$u_z(x, y, z) = |u_z(\mathbf{k})| 2 \sin(\pi z) \cos(k_c x + \phi), \tag{4.24}$$

$$u_x(x, y, z) = \frac{\pi}{k_c} |u_z(\mathbf{k})| 2 \sin(\pi z) \sin(k_c x + \phi), \tag{4.25}$$

where $u_z(\mathbf{k}) = |u_z(\mathbf{k})| \exp(i\phi)$. The stream function ψ for the flow is defined as $\mathbf{u} = -\nabla \times \psi\hat{y}$ that yields $u_z = \partial\psi/\partial x$ using which we derive

$$\psi = -\frac{1}{k_c} \sin(\pi z) \sin(k_x x + \phi) \tag{4.26}$$

We illustrate the above in Fig. 4.2. Note that the roll can be shifted along the x axis by an arbitrary distance due to symmetry of space translation along x. Another important feature of the above solution is that Ra_c is independent of Pr.

Let us study the eigenvectors of A. At neutral equilibrium ($\lambda_+ = 0$), the eigenvalues are 0 and $-(\mathrm{Pr}+1)k^2$, and the corresponding eigenvectors are

$$\left(k^2 1\right); \quad \left(-\mathrm{Pr}k^2 1\right) \tag{4.27}$$

respectively, and they are depicted in Fig. 4.3. Interestingly, the eigenvector corresponding to λ_+ is independent of Pr. Since $\exp(-\lambda_- t) \to 0$, the asymptotic solution is

$$\begin{aligned} \theta(\mathbf{k}, t) &= a_1 & (4.28)\\ u_z(\mathbf{k}, t) &= a_1 k^2. & (4.29) \end{aligned}$$

For Ra just above Ra_c, λ_+ becomes positive, and the eigenvectors would be approximately in the same direction as shown in Fig. 4.3. The solution $u_z(\mathbf{k}, t), \theta(\mathbf{k}, t) \sim \exp(\lambda_+ t)$ grows with time.

The solution for the special case of $\mathrm{Pr} = 0$ is quite interesting. The equations for this case are

$$\begin{aligned} \frac{d}{dt} u_z(\mathbf{k}) &= 0 & (4.30)\\ \frac{d}{dt} \theta(\mathbf{k}) &= u_z(\mathbf{k}) - k^2 \theta(\mathbf{k}) & (4.31) \end{aligned}$$

whose solution is

$$\begin{aligned} u_z(\mathbf{k}, t) &= c_1, & (4.32)\\ \theta(\mathbf{k}, t) &= \frac{c_1}{k^2} + c_2 \exp(-k^2 t) \to \frac{c_1}{k^2}. & (4.33) \end{aligned}$$

Thus, the system admits constant solution for $\mathrm{Pr} = 0$. The solution does not grow with time.

Note that the growing solution saturates due to nonlinearity.